Journal of Hydrology 603 (2021) 126996

Contents lists available at ScienceDirect

Journal of Hydrology

journal homepage: www.elsevier.com/locate/jhydrol

Changes in rainfall erosivity over mainland China under stabilized 1.5 ℃ and 2 ℃ warming futures

Donghuan Li [a,c], Youcun Qi [a,c,*], Tianjun Zhou [b,c,d]

[a] Key Laboratory of Water Cycle and Related Land Surface Processes, Institute of Geographic Sciences and Natural Resources Research, Chinese Academy of Sciences, Beijing, China
[b] LASG, Institute of Atmospheric Physics, Chinese Academy of Science, Beijing, China
[c] University of Chinese Academy of Sciences, Beijing, China
[d] CAS Center for Excellence in Tibetan Plateau Earth Sciences, Chinese Academy of Sciences (CAS), Beijing, China

ARTICLE INFO

Keywords:
Rainfall erosivity
1.5 °C and 2 °C
CESM low-warming
Avoided impact
Simulation

ABSTRACT

Soil erosion is one of the major threats to the environment and agriculture in the world and rainfall erosivity is the most active factor to lead changes in soil erosion. Here, we use statistically downscaled, bias-corrected Community Earth System Model (CESM) low-warming simulations to investigate the future changes in rainfall erosivity in mainland China under the Paris Agreement global warming targets. The downscaled simulations evidently outperform the original CESM simulations in capturing the spatial distribution, magnitudes and annual cycle of rainfall erosivity in China in the present day (1986–2005). The rainfall erosivity will be significantly increased in most regions of China under the 1.5 °C and 2 °C warming targets and the regional mean increases are approximately 33% and 40%, respectively. In addition, the corresponding increases are even larger than 60% and 75%, respectively, in a quarter of mainland China. The increase in rainfall erosivity is resulted from the joint contributions of increases in frequency and intensity of erosive rainfall. However, it is dominated by the increase in the frequency. Compared with annual rainfall amount, the future warming will bring a four times greater impact on the soil erosion potentially caused by rainfall. Limiting global warming to 1.5 °C instead of 2 °C would reduce 17% of the increase in rainfall erosivity in China. For grain producing areas like Sichuan Basin, the middle and lower reaches of Yangtze River and South China, the values are approximately 20%. The future warming will significantly increase the potential risk of soil loss in China, and it is beneficial to relief this risk if the global warming is limited to 1.5 °C rather than 2 °C.

1. Introduction

Soil erosion is one of the major threats to the environment and agriculture in the world, and is influenced by multiple factors, such as soil properties, ground slope, vegetation, runoff and rainfall (Pimentel et al., 1995; Lal, 2004; Pimentel, 2006; Wang et al., 2015). Soil erosion is a global problem, and countries in different continents are more or less affected by it (Bridges and Oldeman, 1999; Li and Fang, 2016). During the second half of the 20th century, nearly one-third of the arable land worldwide was lost caused by erosion, and the per capita food productivity has begun to decline (Pimentel et al., 1995). Previous studies suggest that the soil erosion rate higher than 1•t•ha^{-1}•yr^{-1} could lead to irreversible effects to soil over 50 to 100 years (Jones et al., 2004; Verheijen et al., 2009). China severely suffers from soil erosion, the Xinjiang and Inner Mongolia are mainly affected by wind erosion, the Tibetan Plateau is mainly affected freeze–thaw erosion and the other regions are mainly affected by water erosion (Liao, 1999; Wang et al., 2016). The average potential erosion rate in China is 1.44 t•ha^{-1}•yr^{-1}, and value in some parts of southwestern China is even larger than 10 t•ha^{-1}•yr^{-1}. (Teng et al., 2019). Therefore, it is necessary to pay attention to the future changes of soil erosion in China.

Many models are applied to quantify the effects of different factors on soil erosion, such as the Universal Soil Loss Equation (USLE; Wischmeier and Smith, 1978), the Revised Universal Soil Loss Equation (RUSLE; Renard et al., 1997), and the revised Universal Soil Loss Equation Version 2 (RUSLE2; USDA-Agricultural Research Service,

* Corresponding author at: Key Laboratory of Water Cycle and Related Land Surface Processes, Institute of Geographic Sciences and Natural Resources Research, Chinese Academy of Sciences, Beijing, China.
E-mail address: Youcun.Qi@igsnrr.ac.cn (Y. Qi).

https://doi.org/10.1016/j.jhydrol.2021.126996

Available online 26 September 2021

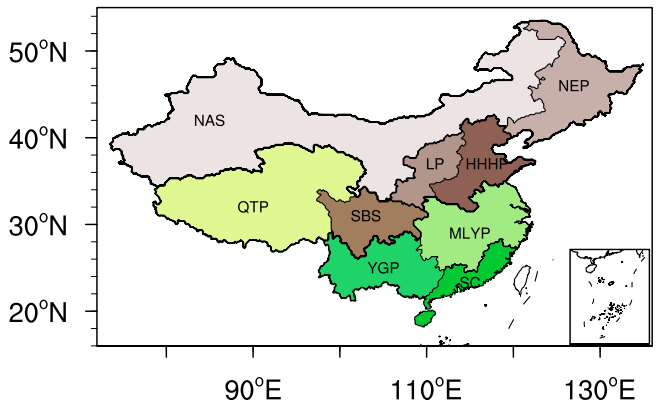

Fig. 1. The division of agricultural regions in mainland China: Northeast China Plain (NEP), Northern arid and semiarid region (NAS), Qinghai Tibet Plateau (QTP), Loess Plateau (LP), Huang-Huai-Hai Plain (HHHP), Middle-lower Yangtze Plain (MLYP), Southern China (SC), Yunnan-Guizhou Plateau (YGP), and Sichuan Basin and surrounding regions (SBS).

2013). These models have been widely applied to investigate soil erosion in different regions worldwide. The soil erodibility, topography, land management, soil conservation practice and rainfall erosivity are considered as the main factors of water erosion in these models (SWCS, 2003). Rainfall erosivity is a good index to characterize the ability of rainfall in leading soil erosion and can be used to indicate the erosion potential (Nearing et al., 2004; Morgan, 2005). As the most active factor in the process of soil erosion, changes in precipitation can directly lead to changes in soil erosion, and the change rate of the latter can be several times of the former. A 4% to 18% increase in precipitation can cause a 31% to 167% increase in soil loss (Zhang, 2007). In addition, increases in the precipitation variability can also lead to the increase in soil erosion (Zhang and Nearing, 2005). Therefore, it is of great importance to investigate the changes in precipitation and rainfall erosivity under the future warming.

Since the industrial revolution, the global averaged temperature has been significantly increased due to the increasing content of greenhouse gases in the atmosphere, and will continue to increase (IPCC, 2013). In recent decades, global warming has had a great impact on climate system, ecological environment and human production and life. Global warming increases the water vapor content in the atmosphere, which can lead to the increases in mean and extreme precipitation (Allan and Soden, 2008; Trenberth et al., 2003; Held and Soden, 2006; O'Gorman and Schneider, 2009; Min et al., 2011; Zhang and Zhou, 2019). The global mean precipitation has been increased in the past century, but the changing pattern of precipitation shows obvious spatial diversity in different regions (Wentz et al., 2007 ; IPCC, 2013). Changes in rainfall erosivity also show spatiotemporal differences. Annual and seasonal rainfall erosivity generally decreased in Elbro Valley of Spain during

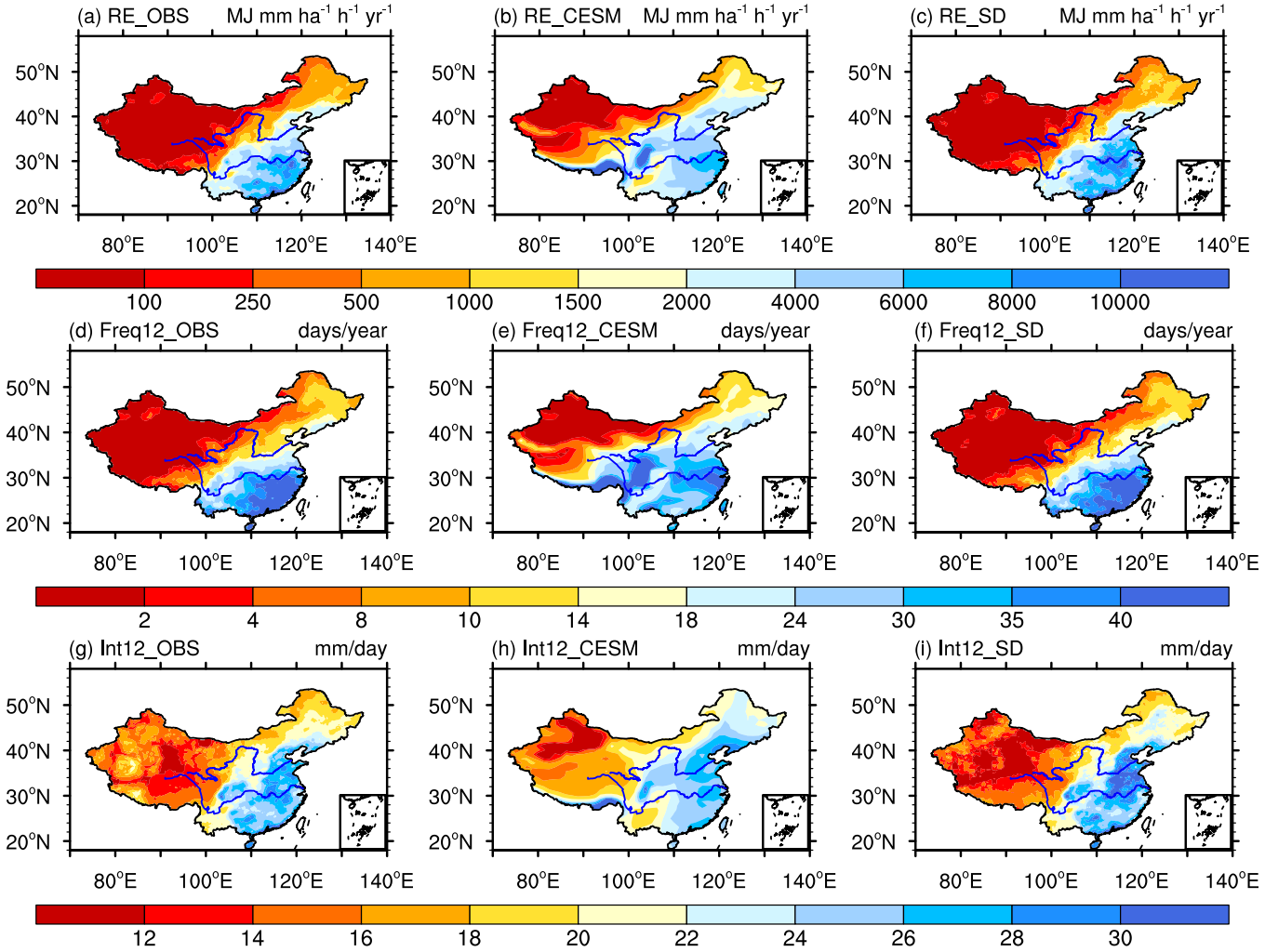

Fig. 2. Spatial distributions of rainfall erosivity (first row) and the frequency (second row) and intensity (third row) of erosive precipitation in 1986–2005. The first, second and third column represents results in the observation, the original CESM ensemble and the statistically downscaled CESM ensemble, respectively.

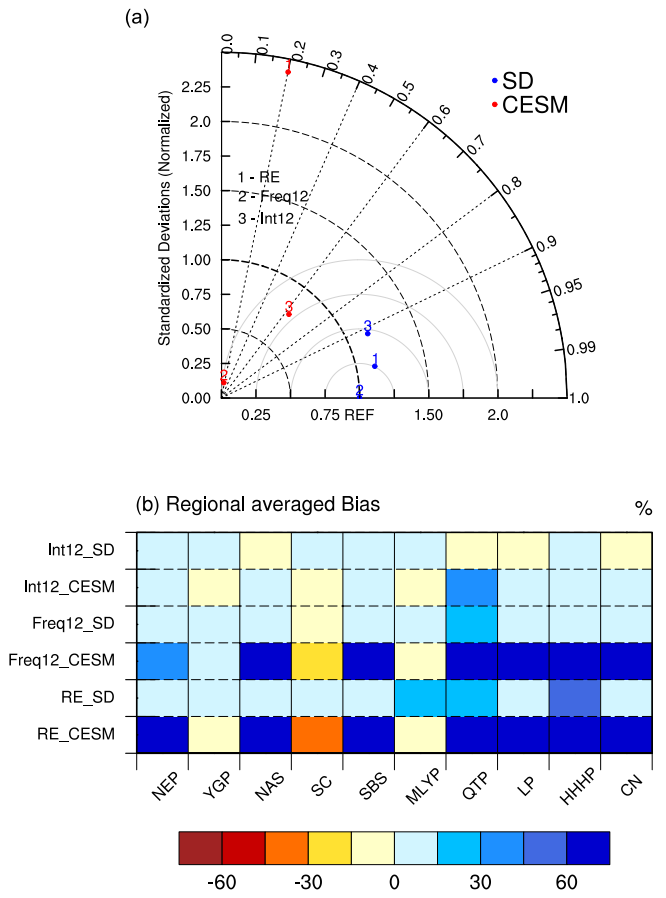

Fig. 3. (a) Taylor diagram for displaying pattern statistics of indices climatology over mainland China simulated by original and downscaled CESM ensemble simulations verified against observations. Different numbers indicate different indices. (b) Regional averaged bias of the mean state for the indices over mainland China (units: %). RE = rainfall erosivity, Int12 = intensity of erosive precipitation, Freq12 = frequency of erosive precipitation, CESM = original CESM ensemble mean, SD = statistically downscaled CESM ensemble mean.

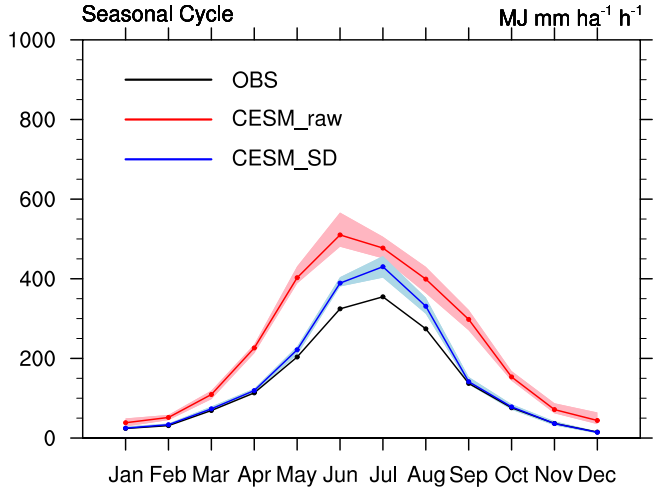

Fig. 4. Seasonal cycle of regional averaged rainfall erosivity in mainland China.

1966–2006 (Angulo-Martínez and Beguería, 2012). Switzerland evidenced a significant increase (decrease) in rainfall erosivity in May to October (February) during 1989–2010 (Meusburger et al., 2012). Rainfall erosivity in mainland China and its water erosion regions experienced an insignificant increase in the past several decades (Liu et al., 2013; Qin et al., 2016).

The future warming will lead to increases in both mean and extreme precipitation in most global land regions and the response of extreme precipitation in the East Asian monsoon region to the future warming is among the greatest across all global monsoon regions (Kitoh et al., 2013; IPCC, 2013; Chen et al. 2020a; Zhang and Zhou, 2020). Rainfall erosivity will increase across central part of India in 2080 s relative to 1961–2001 (Mondal et al., 2016). The central Asia will evidence an increase in rainfall erosivity by 26.6% in the 2070 s under the RCP8.5 scenario relative to 1950–2000 (Duulatov et al., 2019).

In order to mitigate the negative impacts of the future climate change, the Paris Agreement has set a goal of "holding global warming to well below 2 °C and pursuing efforts to limit it to 1.5 °C above pre-industrial levels" (UNFCCC, 2015). Many efforts have been devoted to investigate the climate changes under the 1.5 °C and 2 °C global warming and the avoided climate change impacts owing to the 0.5 °C less warming (e.g., Schleussner et al., 2016; Donnelly et al., 2017; Dosio and Fischer, 2017; King et al., 2017; Li et al., 2018a; Nangombe et al., 2018; Zhang et al., 2018; Zhao and Zhou, 2019; Chen et al., 2020b). However, barely any study has focused on the responses of rainfall erosivity to the warming targets, especially in China under the stabilized 1.5 °C and 2 °C warming targets.

While global climate models (GCMs) are useful tools to project the future change of precipitation and rainfall erosivity, they generally show biases in regional scales due to their relatively low horizontal resolution. To fill in the gap between the low resolution GCM simulations and the desire for finer spatial resolution as well as correction for biases contained in the GCMs, various statistical downscaling methods have been developed (Wilby & Wigley, 1997; Giorgi, 2006; etc.). The statistical downscaling methods use the outputs of the GCMs as predictors for local variables and have been widely used in impact assessments (Maurer & Hidalgo, 2008; Iizumi et al., 2011; Dosio et al., 2012; Gutmann et al., 2014; Li et al., 2018b; Yang et al., 2018). In this study, we have developed a set of statistically downscaled, bias-corrected high resolution projection data based on the Community Earth System Model (CESM) ensemble simulations and investigated the changes in rainfall erosivity in China under the 1.5 °C and 2 °C global warming levels. We have also quantitatively estimated the avoided impacts of the 0.5 °C less warming. In particular, we aim to answer the following questions: (1) whether the downscaled simulations can be used to investigate the rainfall erosivity in China? (2) How will rainfall erosivity change in different regions of China under the 1.5 °C and 2 °C global warming targets? (3) To what extent the changes in rainfall erosivity in China can be avoided if the global warming is limited to 1.5 °C rather than 2 °C?

The remainder of the paper is organized as follows: Section 2 introduces the data and methods used. The main results are shown in Section 3, and Section 4 provides the conclusions of this paper.

2. Data and methods

2.1. CESM low-warming simulation

The CESM low-warming simulations released by the National Center for Atmospheric Research (NCAR) are applied in this study to investigate the rainfall erosivity over mainland China (Kay et al. 2015; Sanderson et al. 2017). This set of model simulations are specifically designed to investigate the climate changes and climate impacts under the 1.5 °C and 2 °C global warming relative to the pre-industrial levels. A set of greenhouse gas emission pathways to obtain long-term global warming that do not exceed 1.5 °C (1.5 °C NE) and 2 °C (2 °C NE) above pre-industrial levels was first produced by a simple Minimal Complexity

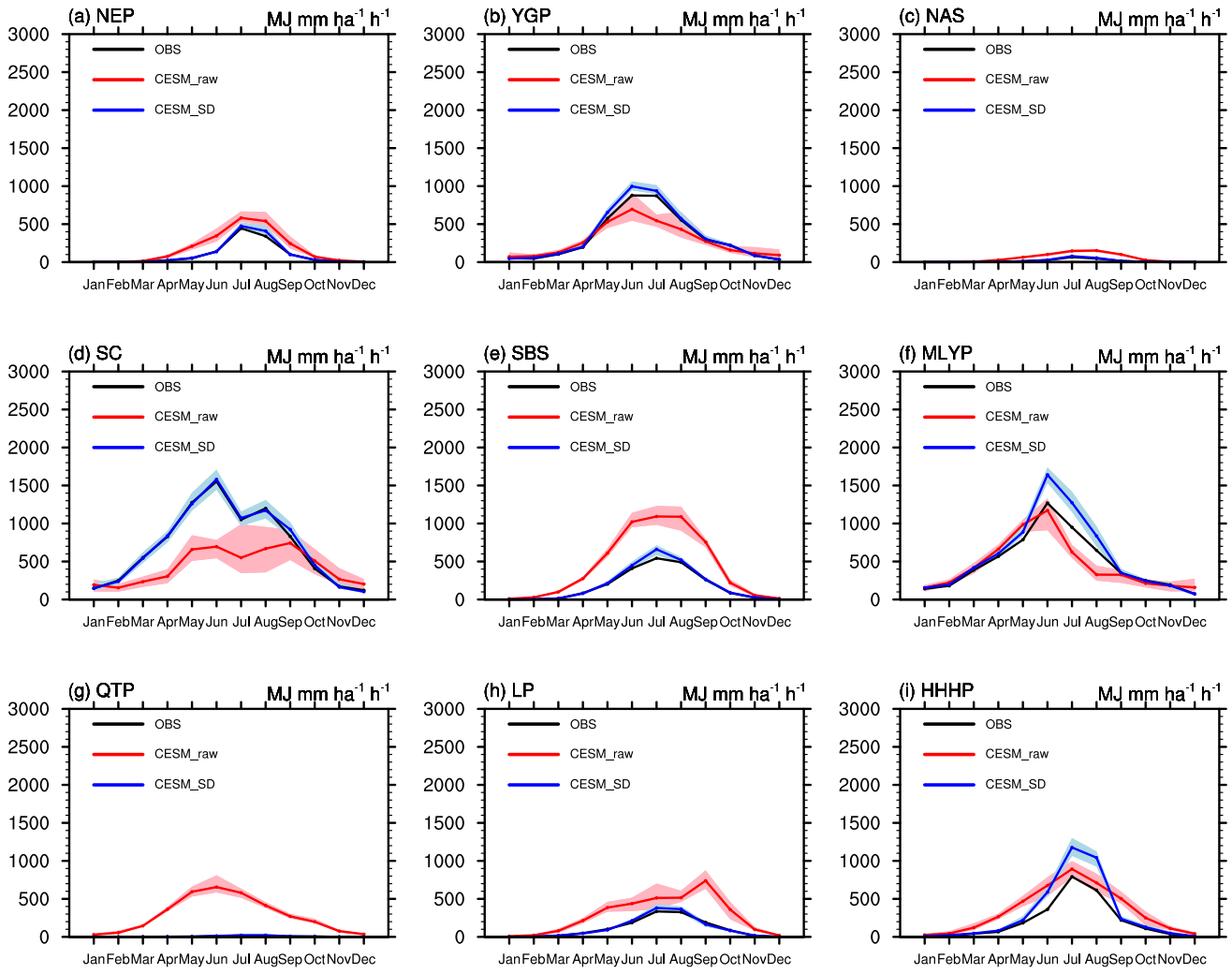

Fig. 5. Seasonal cycle of regional averaged rainfall erosivity in the sub-regions of mainland China.

Earth Simulator (MiCES) model. After that, this set of emission pathways were applied to eleven ensemble members of CESM for the simulation period from 2006 to 2100. Except for greenhouse gas emission pathways, all the other anthropogenic forcings, including land use, aerosol emission and ozone, follow the RCP8.5 scenario throughout the 21st century in the two emission scenarios. In the 1.5 °C NE (2 °C NE) scenario, the global mean temperature reaches 1.5 °C (2 °C) above the pre-industrial levels in 2040 (2090) and stabilizes at this temperature until 2100. The horizontal resolution of the CESM simulation is 1°×1°. For more detailed information of the CESM low-warming simulations, please refer to Sanderson et al. (2017).

2.2. The statistical downscaling method

The statistical downscaling model applied in this study is a regression model (Dettinger et al., 2004). Separate time periods are selected to calibrate and validate the model. In this study, the calibration period is from 1966 to 1985 and the validation period is from 1986 to 2005. The daily precipitation from the CESM simulations is downscaled. The detailed downscaling procedure is as follows: Firstly, for each grid in the observation dataset, the values in the nearest grid in the CESM simulations are set to this certain grid. That means, the horizontal resolution of output of the statistical downscaling model is the same as the observation dataset. Then, the daily precipitation in both the observation dataset and the CESM simulations is sort at each grid for each month of the multiyear during the calibration period. In order to ensure the same numbers of wet events (days with precipitation) in the CESM simulations and the observation, a threshold is set in the CESM simulations if there are more wet events in the simulations. After that, the regression relationship between the wet events in the observation and the simulation are fit by high-order polynomials. This statistical downscaling model has been applied to investigate the climate change in China in previous studies (Dai et al., 2014; Li et al., 2018b).

The credibility of the model is also investigated. Following Salvi et al. (2016), the statistical downscaling model is firstly cross validated by using 1986–2005 as the calibration period and 1966–1985 as the validation period. Then the capability of the statistical downscaling model in capturing the changes in mean precipitation caused by GHG emissions is checked. We use the 2 °C warmer climate as “high GHG emissions period” and the pre-industrial control run as “no anthropogenic GHG emissions period” and the results show that the statistical downscaling model is credible in a changing climate. Please refer to Salvi et al. (2016) for more detailed information of the credibility checking approach.

2.3. Observation data

Daily precipitation from the CN05.1 dataset (Xu et al., 2009; Wu et al., 2013) with a horizontal resolution of 0.25°×0.25° is used to calibrate the statistical downscaling model and to validate the model results. The time period is from 1966 to 2005. The CN05.1 dataset is interpolated from over 2400 observing stations in China and is quality controlled by the China Meteorological Administration (CMA).

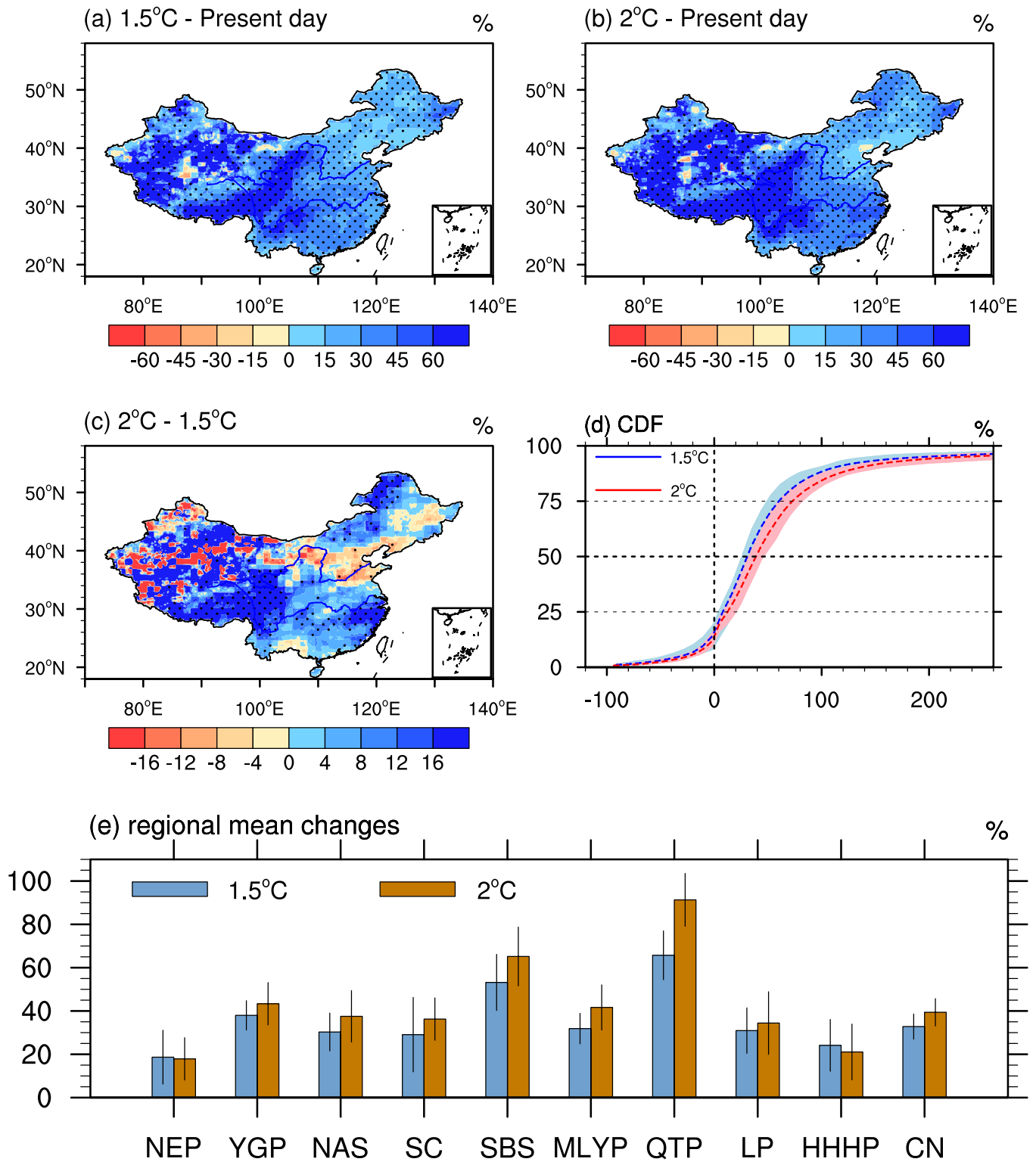

Fig. 6. Relative changes in rainfall erosivity in 2081–2100 relative to 1986–2005 in the (a) 1.5 °C and (b) 2 °C warmer climates. Subplot (c) shows the differences between the 2 °C and 1.5 °C. Dotted areas are statistically significantly different from zero at the 10% level according to Student's *t*-test. Subplot (d) shows CDFs for regional aggregated changes in rainfall erosivity in 2081–2100 relative to 1986–2005. The shaded areas represent the range of one standard deviation across members and the lines represent the multimember mean. Subplot (e) is the regional mean changes in rainfall erosivity in 2081–2100 relative to 1986–2005, and the black sticks over the bars show the range between maximum and minimum values across ensemble members.

2.4. The bias correction method

Considering that absolute threshold is used to define erosive precipitation, a simple bias correction method called multiple local scaling (LS) factor (Casanueva et al., 2016) is applied to further correct the systematic deviation of downscaled precipitation for each season at each grid:

Table 1
Regional mean changes of rainfall erosivity in 2081–2100 relative to 1986–2005 (units: %) in different regions of mainland China. The "_CESM" represents the results in the original CESM projections and "_SD" represents the results in the SD projections. The number in [ ] represents the standard deviation across the ensemble members.

	1.5 °C _CESM	1.5 °C _SD	2 °C _CESM	2 °C _SD
NEP	16 [10]	19 [12]	15 [10]	18 [12]
YGP	30 [6]	38 [7]	37 [6]	43 [7]
NAS	25 [9]	30 [9]	29 [9]	38 [9]
SC	22 [14]	29 [17]	30 [14]	36 [17]
SBS	40 [7]	53 [13]	51 [7]	65 [13]
MLYP	26 [6]	32 [7]	37 [6]	42 [7]
QTP	23 [7]	66 [11]	31 [7]	91 [11]
LP	21 [9]	31 [11]	27 [9]	34 [11]
HHHP	18 [7]	24 [12]	20 [7]	21 [12]
CN	25 [3]	33 [6]	33 [3]	39 [6]

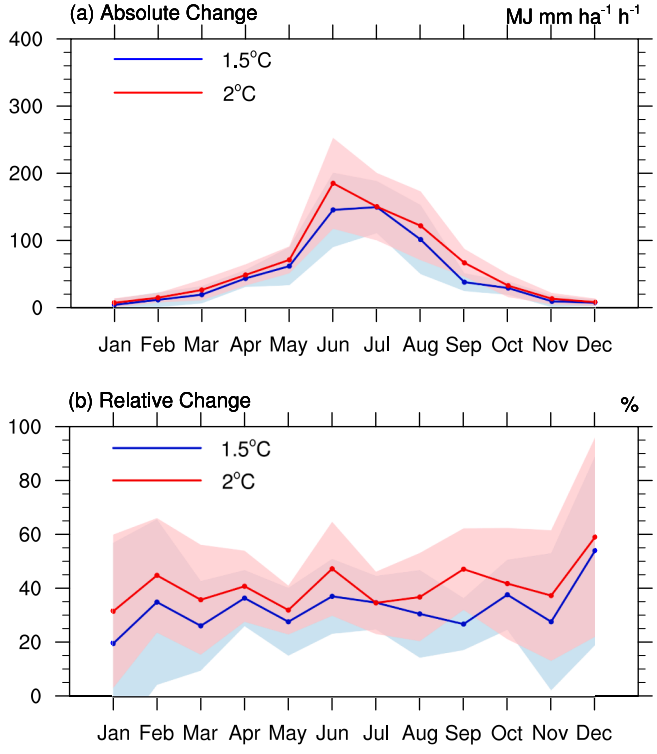

Fig. 7. (a) Absolute and (b) relative regional mean changes in rainfall erosivity over mainland China in 2081–2100 relative to 1986–2005 in the (a) 1.5 °C and (b) 2 °C warmer climates. The shaded areas represent the range of one standard deviation across members and the lines represent the multi-member mean.

$$RR_{LS} = RR_{DS}\frac{RM_{OBS}}{RM_{DS}} \quad (1)$$

where RR_{DS} is the daily downscaled precipitation, respectively. RM_{OBS} and RM_{DS} are the seasonal mean observed and downscaled precipitation, respectively. $\frac{RM_{OBS}}{RM_{DS}}$ is the scaling factor and applied in both the present day simulation and future projections.

2.5. Rainfall erosivity factor (R-factor)

Due to the lack of high time resolution precipitation data, daily precipitation is widely used to calculate the R-factor (e.g. Hoyos et al., 2005; Angulo-Martínez et al., 2009; Angulo-Martínez and Beguería, 2012; Zhu and Yu, 2015). The method proposed by Zhang et al. (2002) is applied in this study. This method has been widely used to calculate R-factor in different regions of China (Men et al., 2008; Huang et al., 2013; Ma et al., 2014; Yang and Lu, 2015; Qin et al., 2016). The calculation formula is as follows:

$$R_i = \alpha\sum_{j=1}^{k}(D_j)^{\beta} \quad (2)$$

where R_i is the rainfall erosivity in the ith half-month of the year, and its unit is MJ•mm•ha^{-1}•h^{-1}. D_j is the effective rainfall for day j in this certain half-month, that means $D_j$is set to the actual rainfall if the rainfall in a day is larger than 12 mm (the threshold of erosive precipitation in this study), otherwise, $D_j$is set to zero. k is the number of days in this half-month. α and β are parameters calculated based on continuous rainfall data series with a high time resolution and the empirical formulas are as follows:

$$\beta = 0.8363 + 18.144{P_{d12}}^{-1} + 24.455{P_{y12}}^{-1} \quad (3)$$

$$\alpha = 21.586\beta^{-7.1891} \quad (4)$$

P_{d12} and P_{y12} represent the average daily and annual rainfall for erosive precipitation days, respectively. This daily rainfall erosivity model can well estimate the climatology of rainfall erosivity and its seasonal distribution, especially in the regions with abundant precipitation. However, the model may underestimate the erosion caused by extreme storm (Zhang et al., 2002).

2.6. Time periods and sub-regions

The period from 1986 to 2005 is referred as the present day and the period from 2081 to 2100 in the two low-warming scenarios represent the 1.5 °C and 2 °C global warming levels above the pre-industrial levels.

The study region is classified into nine sub-regions according to the agricultural regions in mainland China (Fig. 1): Northeast China Plain (NEP), Northern arid and semiarid region (NAS), Qinghai Tibet Plateau (QTP), Loess Plateau (LP), Huang-Huai-Hai Plain (HHHP), Middle-lower Yangtze Plain (MLYP), Southern China (SC), Yunnan-Guizhou Plateau (YGP), and Sichuan Basin and surrounding regions (SBS).

2.7. Definition of indices and avoided impact

Three indices are used in this study. The erosive precipitation day defined in this study is a day when the daily precipitation is larger than 12 mm. Freq12 and Int12 are the annual frequency and annual mean intensity of erosive precipitation. Besides, RE represents rainfall erosivity in the following parts.

The impact of rainfall erosivity that avoided at 1.5 °C compared with the 2 °C warming level is calculated using the formula below (Li et al., 2018a):

$$\mathrm{AI} = \frac{C_{2.0} - C_{1.5}}{C_{2.0}} \times 100\% \quad (5)$$

where AI is the avoided impact. $C_{1.5}$ and $C_{2.0}$ represent the changes of rainfall erosivity at the 1.5 °C and 2 °C warming levels relative to the present day.

3. Results

3.1. Validation of the model simulations in the present day

We first evaluate the model performance. In the present day, the annual rainfall erosivity decreases from the southeast to the northwest of China in the observation, like that of the annual precipitation, ranging from higher than 10,000 MJ•mm•ha^{-1}•h^{-1}•a^{-1} to lower than 50 MJ•mm•ha^{-1}•h^{-1}•a^{-1} (Fig. 2a). For the regional mean of the sub-regions, it is highest in SC and lowest in NAS (Figs. 1 and 2a). The Freq12 also decreases from the southeast to the northwest of China, from larger than

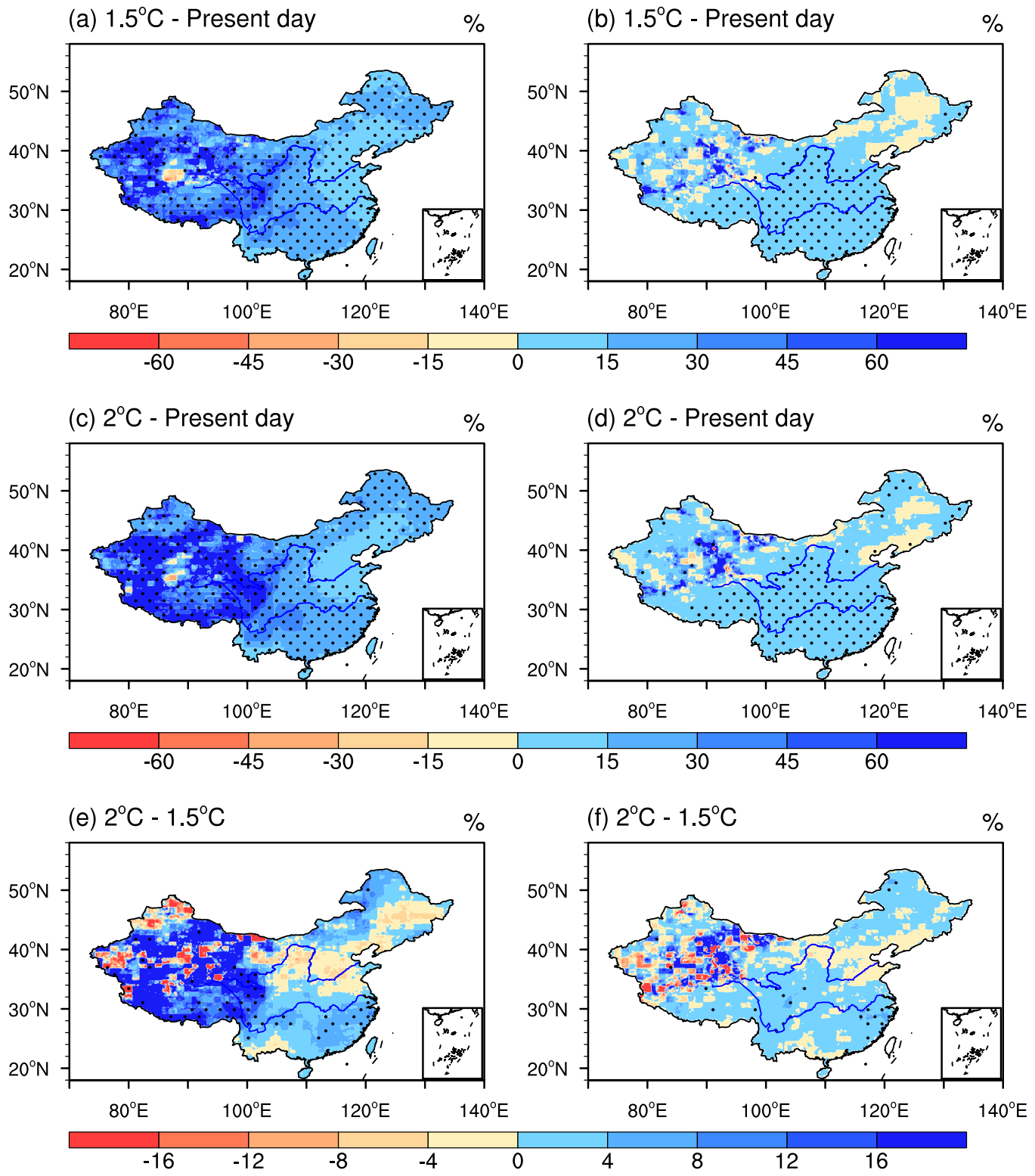

Fig. 8. Relative changes in the frequency of erosive precipitation in 2081–2100 relative to 1986–2005 in the (a) 1.5 °C and (c) 2 °C warmer climates. Subplot (e) shows the differences between the 2 °C and 1.5 °C. Subplots (b), (d) and (f) correspond to subplots (a), (c) and (e), but for changes in the intensity of erosive precipitation. Dotted areas are statistically significantly different from zero at the 10% level according to Student's *t*-test.

40 days per year to smaller than 2 days per year (Fig. 2b). Generally, the Int12 also shows similar spatial distribution with the RE (Fig. 1c), however, the central value is located between the Yangtze River and the Yellow River in eastern China. Hence, the spatial distribution of RE over mainland China is the combined results of frequency and intensity of erosive precipitation.

The original CESM low-warming simulations (hereafter the CESM) can roughly capture the spatial distribution and magnitudes of RE in mainland China, but overestimate RE in most parts of western China and underestimate it in most parts of eastern China (Fig. 2d). Therefore, the gradient of RE from southeast to northwest China is smaller in the CESM than in the observation. This bias is reflected in both the frequency and

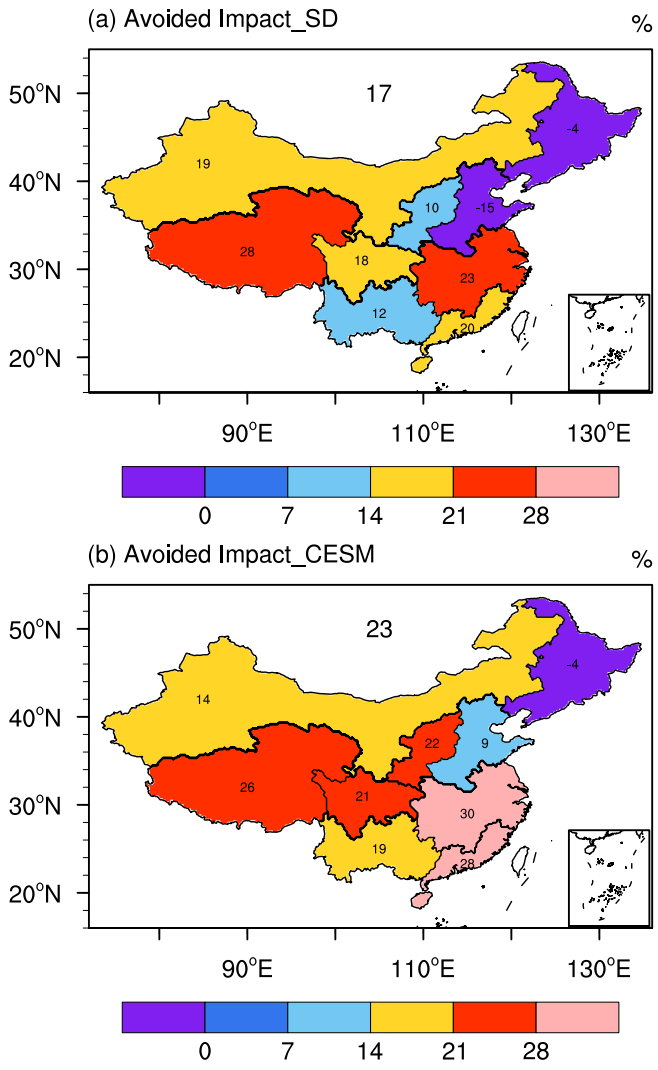

Fig. 9. Changes in rainfall erosivity avoided over mainland China and its sub-regions in the 1.5℃ warmer climate compared with the 2℃ warmer climate in (a) the SD and (b) the original CESM.

intensity of erosive precipitation, especially the frequency (Fig. 2e and f). The statistical downscaling simulations (hereafter the SD) show evident improvement compared with the CESM in capturing the climatology characteristics of RE in mainland China (Fig. 2g). Both the spatial distribution and the magnitude are more close to the observation. Similar improvement is evident in the frequency and intensity of erosive precipitation in the SD (Fig. 2h and i).

We further quantitatively measure the model skill (Fig. 3). Taylor diagram is used to evaluate the performance of the SD and the CESM in terms of pattern correlations, the root-mean-square differences, and the ratios of spatial variations in the simulated and observed values of the RE, Freq12 and Int12 (the observation is used as the reference). In the CESM, the pattern correlation of RE is around 0.2 and the ratio of spatial standard deviation is more than 2.0 (Fig. 3a). The regional averaged biases of RE in most sub-regions are larger than 30% and even 60% (Fig. 3b). The biases of RE in the CESM are mainly caused by the biases in the Freq12. The pattern correlation is around 0.2 and the regional averaged biases are larger than 60% in most sub-regions. Differently, the biases of Int12 are relatively small. The pattern correlation is around 0.6, and the ratio of spatial standard deviations is approximately 0.75 (Fig. 3a). In addition, the regional averaged biases are within ± 15% in most sub-regions (Fig. 3b). The SD outperforms the CESM for all the three indices, with pattern correlations larger than 0.9 and the ratios of spatial standard deviations close to 1.0, especially for Freq12 (Fig. 3a). The regional averaged biases are also smaller in the SD, with values within ± 15% for the three indices in most sub-regions (Fig. 3b).

The regional mean RE over mainland China shows obvious annual cycle in the present day, with peak values of about 360 MJ•mm•ha^{-1}•h^{-1} occurring in July (Fig. 4). The annual cycle of RE in mainland China can be roughly reproduced in the CESM, but is overestimated throughout the year. Besides, the peak values of RE occurs in June. Compared with the CESM, the SD exhibits obvious improvements in reproducing the annual cycle of regional mean RE in mainland China, with the overestimation evidently reduced and the peak value occurring in July (Fig. 4). There are certain differences in the annual cycle of RE in different sub-regions, but the peak values all occur in summer (Fig. 5). Consistent with the results shown above (Figs. 2 and 3), The CESM underestimates the RE in southern China and overestimates the RE in northern China (Fig. 5). In addition, these biases exist throughout the year. The SD performs well in most sub-regions, and only overestimates the RE in MLYP and HHHP in summer.

In general, compared with the original CESM simulations, the SD performs better in reproducing the characteristics of rainfall erosivity and its important determinants, the frequency and intensity of erosive precipitation, in the present day in mainland China. However, there are still some biases in the SD. The reason is that, the statistical downscaling method applied in this study can help to obtain more detailed spatial distribution of precipitation and reduce the biases of climatic state of precipitation in the global model. After statistical downscaling, the biases of precipitation with different intensity will be reduced but not fully eliminated. In the following analysis, the SD is applied to investigate the changes in rainfall erosivity and erosive precipitation in mainland China at the 1.5 °C and 2 °C global warming levels.

3.2. *Future projections of rainfall erosivity*

We first examine the changes in annual rainfall erosivity. The changing patterns of RE in the two warmer climates are similar. Compared with the present day, the annual rainfall erosivity will increase significantly in most areas of mainland China at the 1.5 °C and 2 °C global warming levels, with the large values occurring in central China and the southern edge of the Tibetan Plateau (Fig. 6a and b). Compared with the 1.5 °C warmer climate, the extra 0.5 °C warming in the 2 °C warmer climate will significantly lead to larger RE in most parts of China, except some parts of North China (Fig. 6c). The most obvious increases (larger than 16%) lie in the Sichuan Basin and parts of Southeast China, two of the important grain producing areas in China.

The cumulative density function (CDF) is applied to quantitatively analyze the changes of RE in China. Individual grid cells are weighted by their area. The CDFs can apparently exhibit both the median change of RE in China and the changes in small fractions. Compared with the present day, about half landmass of mainland China will experience a RE increase of 30% and 40% in the 1.5 °C and 2 °C warmer climates, respectively. The corresponding increases will be even larger than 60% and 75%, respectively, in a quarter of mainland China (Fig. 6d). Regional mean changes in RE in mainland China are approximately 33% and 40% under the 1.5 °C and 2 °C global warming, respectively, about four times larger than the corresponding increase in precipitation (5.5% and 7.3% under the 1.5 °C and 2 °C global warming, respectively; Li et al., 2019). QTP and SBS will experience larger RE increase than other sub-regions (Fig. 6d). Compared with the original CESM projection, the increasing magnitudes of rainfall erosivity in the SD are larger in all the nine subregions in the two warmer climates and the differences between these two sets of simulations are largest in the Tibetan Plateau (Table 1). The possible reason for these differences is that the SD can better capture the spatial distributions and magnitudes of frequency and intensity of erosive precipitation.

Seasonal features of changes in RE over China are further investigated (Fig. 7). We first examine the absolute changes of RE. In the two

warmer climates, the RE will increase throughout the year, with peak values occurring in summer months (Fig. 7a). The increases in RE caused by extra 0.5 °C warming in the 2 °C warmer climate mainly appear in June to September (Fig. 7a). Distinctly, the magnitudes of relative changes in RE among different months are comparable, around 30% and 40% in the 1.5 °C and 2 °C warmer climates, respectively (Fig. 7b). Therefore, the future warming basically will not change the seasonal distributions of RE in mainland China in terms of regional mean, but lead to an overall RE increase throughout the year.

Freq12 will increase in most parts of mainland China in the warming future (Fig. 8a and b). The changing patterns of Freq12 in the two warmer climates are similar with those of RE (Figs. 6 and 8). Int12 will also increase under the future warming, but the magnitudes are obviously smaller than those of increase in Freq12 (Fig. 8d and e). Therefore, increases in the frequency of erosive precipitation contribute more to the increases in RE in the warming future than the intensity of erosive precipitation. It is worth noting that the increasing magnitudes of RE are evidently larger than both Freq12 and Int12.

We use formula (5) to quantify the impacts of increased RE avoided if the global warming is controlled well below 1.5 °C rather than 2 °C (Fig. 9). In the SD, compared with the 2 °C warmer climate, the half-degree less warming in the 1.5 °C warmer climate will help to reduce 17% of the increase in RE over mainland China. Except NEP and HHHP, the increases of RE will be avoided in most sub-regions of mainland, from 10% in LP to 28% in QTP. For major grain producing areas like SBS, MLYP and SC, the avoided increase in RE are approximately 20%. The results in the original CESM are comparable with or a little larger than those in the SD in most subregions. The half-degree less warming in the 1.5 °C warmer climate will help to reduce 23% of the increase in RE over mainland China.

4. Conclusion and summary

The CESM low-warming simulations released by NCAR are specifically designed to investigate climate change and climate impacts of 1.5 °C and 2 °C global warming above the pre-industrial levels. In this study, statistically downscaled and bias-corrected CESM low-warming ensemble simulations are developed and applied to investigate the changes in rainfall erosivity and erosive precipitation in mainland China at the 1.5 °C and 2 °C global warming levels. The main conclusions are summarized as follows:

(1) Compared with the original CESM low-warming simulations, the downscaled simulations show much better performance in reproducing the spatial distributions and annual cycle of RE in mainland China. The pattern correlations of RE, Freq12 and Int12 are larger than 0.9, and the regional mean biases of the three indices are within ± 15% in most sub-regions.
(2) The RE will evidence a robust increase in mainland China, with larger increasing magnitudes under 2 °C compared with 1.5 °C warming target in most sub-regions. The increasing magnitudes are larger than 60% and 75% in a quarter of mainland China at the 1.5 °C and 2 °C global warming levels, respectively. The absolute increases of regional mean RE over China show obvious seasonality, with peak values occurring in summer. However, the relative increases of RE among different months are comparable, around 30% and 40% in the 1.5 °C and 2 °C warmer climates, respectively. The increasing magnitudes of rainfall erosivity in the original CESM are a little smaller than those in the SD.
(3) The increase in RE is resulted from the joint contributions of increases in Freq12 and Int12. The spatial distribution of increases in RE is dominated by that of the increase in Freq12. Differently, the increases in the intensity of erosive precipitation are relatively uniform in mainland China in the two stabilized warming conditions. In addition, the changing magnitudes of RE are much larger than those of annual precipitation or the frequency and intensity of erosive precipitation. The increasing magnitudes of regional mean RE in mainland China are about four times larger than the corresponding increase in annual precipitation in the two warmer climates. Therefore, compared with annual rainfall amount, the future warming will bring a greater impact on the soil erosion potential caused by rainfall.
(4) Compared with the 2 °C warmer climate, the 0.5 °C less warming in the 1.5 °C warmer climate will help to avoid 17% of the increase in rainfall erosivity in mainland China, with greatest reduction of 28% occurring in QTP. For grain producing areas like SBS, MLYP and SC, the values are approximately 20%. The correspond values in the original CESM are comparable with or a little larger than those in the SD in most subregions. The half-degree less warming in the 1.5 °C warmer climate will help to reduce 23% of the increase in RE over mainland China. Our analysis suggests that the future warming will significantly increase the potential risk of soil erosion in mainland China, and controlling the global warming to 1.5 °C above the pre-industrial levels rather than 2 °C is beneficial to reduce this risk.

Rainfall erosivity is directly associated with the intensity, frequency, and amount of precipitation. Different models and methods have been applied to investigate the changes of these different characteristics of precipitation over East Asia under the 1.5 °C and 2 °C warming conditions, including the regional climate models (Li et al., 2018c), the Coupled Model Intercomparison Project Phase 5 (CMIP5) models (Zhou et al., 2019) and the stand-alone AGCM simulations of the HAPPI (Half-a-degree Additional warming, Prognosis and Projected Impacts) project (Lee et al., 2018). The results are qualitatively consistent but quantitatively different among these models and methods (Li et al., 2019). The results of this study are only derived from one set of coupled low-warming simulations, and this may lead to uncertainties in the projection of rainfall erosivity. Further investigation should be done in the future work due to the model dependence of the results presented here. Moreover, climate projections are scenario-dependent. A new set of future scenarios, namely the combined scenarios of the Shared Socioeconomic Pathways (SSPs) and Representative Concentration Pathways (RCPs) are designed and applied to the CMIP6 models (O'Neill et al., 2016). The changes of rainfall erosivity under these new scenarios should be also investigated.

Changes of rainfall erosivity is a good indicator of the changes of soil erosion potential in the warming future. It is worth noting that, in addition to the changes of rainfall, changes of land use/land cover (LULC) also have large impacts on the changes of soil erosion. For example, the conversion of naturally vegetated areas for agricultural uses may intensify soil erosion (Tarolli and Sofia, 2016; Yang and Lu, 2018) and grain for green can effectively decrease the soil erosion (Deng et al., 2012). There are large uncertainties in the future greenhouse gas emissions and land uses. Statistically explore their relative contributions to the changes of soil erosion is of great importance to the adaptation and mitigation policies (Borrelli et al., 2020; Saha and Ghosh, 2020). Borrelli et al. (2020) uses three alternative (2.6, 4.5, and 8.5) Shared Socioeconomic Pathway and Representative Concentration Pathway (SSP-RCP) scenarios to investigates the impacts of land use and climate change on the global erosion by water. They indicate that the future changes of soil erosion are dominated by climate change and the contributions of socioeconomic developments impacting land use to changes in water erosion are relatively small. Similarly, changes of surface hydrology of the Ganga river basin are also dominated by the climate change mitigation pathways (Saha and Ghosh, 2020). The relative contributions of changes in rainfall and land use to the changes of soil erosion in China in the 1.5 °C and 2 °C warmer climates are still not clear and should be further investigated in the future work.

Author contributions

Youcun Qi and Donghuan Li managed the research. Donghuan Li and Tianjun Zhou collected and prepared the raw data. Donghuan Li produced figures and wrote the paper. Youcun Qi and Tianjun Zhou helped to polish the paper.

Declaration of Competing Interest

The authors declare that they have no known competing financial interests or personal relationships that could have appeared to influence the work reported in this paper.

Acknowledgments

Major funding for this research was provided under Strategic Priority Research Program of Chinese Academy of Sciences (Grant No. XDA2006040101), and Hundred Talent Program.

References

Allan, R.P., Soden, B.J., 2008. Atmospheric warming and the amplification of precipitation extremes. Science 321 (5895), 1481–1484.
Angulo-Martínez, M., Beguería, S., 2012. Trends in rainfall erosivity in NE Spain at annual, seasonal and daily scales, 1955–2006. Hydrol. Earth Syst. Sci. 16 (10), 3551–3559.
Angulo-Martínez, M., López-Vicente, M., Vicente-Serrano, S.M., Beguería, S., 2009. Mapping rainfall erosivity at a regional scale: a comparison of interpolation methods in the Ebro Basin (NE Spain). Hydrol. Earth Syst. Sci. 13 (10), 1907–1920.
Borrelli, P., Robinson, D.A., Panagos, P., Lugato, E., Yang, J.E., Alewell, C., Ballabio, C., 2020. Land use and climate change impacts on global soil erosion by water (2015–2070). Proc. Natl. Acad. Sci. 117 (36), 21994–22001.
Bridges, E.M., Oldeman, L.R., 1999. Global assessment of human-induced soil degradation. Arid Soil Res. Rehabil. 13 (4), 319–325.
Casanueva, A., Herrera, S., Fernández, J., Gutiérrez, J.M., 2016. Towards a fair comparison of statistical and dynamical downscaling in the framework of the EURO-CORDEX initiative. Clim. Change 137 (3), 411–426.
Chen, Z., Zhou, T., Zhang, L., Chen, X., Zhang, W., Jiang, J., 2020a. Global land monsoon precipitation changes in CMIP6 projections. Geophys. Res. Lett. 47 (14) e2019GL086902.
Chen, Z., Zhou, T., Zhang, W., Li, P., Zhao, S., 2020b. Projected changes in the annual range of precipitation under stabilized 1.5 C and 2.0 C warming futures. Earth's Fut. 8 (9) e2019EF001435.
Dai, Y.F., Liu, Y.M., Jin, J.M., 2014. Statistical downscaling of FGOALS-s2 projected precipitation in Eastern China. Atmos. Oceanic Sci. Lett. 7 (5), 388–394.
Deng, L., Shangguan, Z., Li, R., 2012. Effects of the grain-for-green program on soil erosion in China. Int. J. Sedim. Res. 27 (1), 120–127.
Dettinger, M.D., Cayan, D.R., Meyer, M.K., Jeton, A.E., 2004. Simulated hydrologic responses to climate variations and change in the Merced, Carson, and American River basins, Sierra Nevada, California, 1900–2099. Clim. Change 62 (1), 283–317.
Donnelly, C., Greuell, W., Andersson, J., Gerten, D., Pisacane, G., Roudier, P., Ludwig, F., 2017. Impacts of climate change on European hydrology at 1.5, 2 and 3 degrees mean global warming above pre-industrial level. Clim. Change 143 (1), 13–26.
Dosio, A., Fischer, E.M., 2018. Will half a degree make a difference? Robust projections of indices of mean and extreme climate in Europe under 1.5 C, 2 C, and 3 C global warming. Geophys. Res. Lett. 45 (2), 935–944.
Dosio, A., Paruolo, P., Rojas, R., 2012. Bias correction of the ENSEMBLES high resolution climate change projections for use by impact models: Analysis of the climate change signal. J. Geophys. Res.: Atmos. 117 (D17).
Duulatov, E., Chen, X., Amanambu, A.C., Ochege, F.U., Orozbaev, R., Issanova, G., Omurakunova, G., 2019. Projected rainfall erosivity over Central Asia based on CMIP5 climate models. Water 11 (5), 897.
Giorgi, F., 2006. Regional climate modeling: Status and perspectives. J. de Physique IV (Proceedings) 139, 101–118. https://doi.org/10.1051/jp4:2006139008.
Gutmann, E., Pruitt, T., Clark, M.P., Brekke, L., Arnold, J.R., Raff, D.A., Rasmussen, R.M., 2014. An intercomparison of statistical downscaling methods used for water resource assessments in the U nited S tates. Water Resour. Res. 50 (9), 7167–7186.
Held, I.M., Soden, B.J., 2006. Robust responses of the hydrological cycle to global warming. J. Clim. 19 (21), 5686–5699.
Hoyos, N., Waylen, P.R., Jaramillo, Á., 2005. Seasonal and spatial patterns of erosivity in a tropical watershed of the Colombian Andes. J. Hydrol. 314 (1–4), 177–191.
Huang, J., Zhang, J., Zhang, Z., Xu, C.Y., 2013. Spatial and temporal variations in rainfall erosivity during 1960–2005 in the Yangtze River basin. Stoch. Env. Res. Risk Assess. 27 (2), 337–351.
Iizumi, T., Nishimori, M., Dairaku, K., Adachi, S.A., Yokozawa, M., 2011. Evaluation and intercomparison of downscaled daily precipitation indices over Japan in present-day climate: Strengths and weaknesses of dynamical and bias correction-type statistical downscaling methods. J. Geophys. Res.: Atmos. 116 (D1).
IPCC. Climate Change 2013: The Physical Science Basis. Cambridge, UK, and New York, USA: Cambridge University Press, 2013.
Jones, R. J., Le Bissonnais, Y., Bazzoffi, P., Sanchez Diaz, J., Düwel, O., Loj, G., Yordanov, Y., 2004. Nature and extent of soil erosion in Europe. Reports of the technical working groups established under the thematic strategy for soil protection, 2.
Kay, J.E., Deser, C., Phillips, A., Mai, A., Hannay, C., Strand, G., Vertenstein, M., 2015. The Community Earth System Model (CESM) large ensemble project: A community resource for studying climate change in the presence of internal climate variability. Bull. Am. Meteorol. Soc. 96 (8), 1333–1349.
King, A.D., Karoly, D.J., Henley, B.J., 2017. Australian climate extremes at 1.5 C and 2 C of global warming. Nature. Clim. Change 7 (6), 412–416.
Kitoh, A., Endo, H., Krishna Kumar, K., Cavalcanti, I.F., Goswami, P., Zhou, T., 2013. Monsoons in a changing world: A regional perspective in a global context. Journal of Geophysical Research: Atmospheres 118 (8), 3053–3065.
Lal, R., 2004. Soil carbon sequestration impacts on global climate change and food security. Science 304 (5677), 1623–1627.
Lee, D., Min, S.K., Fischer, E., Shiogama, H., Bethke, I., Lierhammer, L., Scinocca, J.F., 2018. Impacts of half a degree additional warming on the Asian summer monsoon rainfall characteristics. Environ. Res. Lett. 13 (4), 044033.
Li, Z., Fang, H., 2016. Impacts of climate change on water erosion: A review. Earth Science Reviews.
Li, D., Zhou, T., Zhang, W., 2019. Extreme precipitation over East Asia under 1.5° C and 2° C global warming targets: a comparison of stabilized and overshoot projections. Environ. Res. Commun. 1 (8), 085002.
Li, D., Zhou, T., Zou, L., Zhang, W., Zhang, L., 2018a. Extreme high-temperature events over East Asia in 1.5° C and 2° C warmer futures: analysis of NCAR CESM low-warming experiments. Geophys. Res. Lett. 45 (3), 1541–1550.
Li, D., Zou, L., Zhou, T., 2018b. Extreme climate event changes in China in the 1.5 and 2 C warmer climates: results from statistical and dynamical downscaling. J. Geophys. Res.: Atmos. 123 (18), 10–215.
Li, H., Chen, H., Wang, H., Yu, E., 2018c. Future precipitation changes over China under 1.5 C and 2.0 C global warming targets by using CORDEX regional climate models. Sci. Total Environ. 640, 543–554.
Liao, K., 1999. The national physical atlas of china. SinoMaps Press, Beijing, China (in Chinese).
Liu, B.T., Tao, H.P., Song, C.F., Guo, B., Shi, Z., Zhang, C., Kong, B., He, B., 2013. Temporal and spatial variations of rainfall erosivity in China during 1960 to 2009. Geogr. Res. 32 (2), 245–256 (In Chinese with English Abstract).
Ma, X., He, Y., Xu, J., van Noordwijk, M., Lu, X., 2014. Spatial and temporal variation in rainfall erosivity in a Himalayan watershed. Catena 121, 248–259.
Maurer, E.P., Hidalgo, H.G., 2008. Utility of daily vs. monthly large-scale climate data: An intercomparison of two statistical downscaling methods. Hydrol. Earth Syst. Sci. Discuss. 4 (5), 3413–3440.
Men, M., Yu, Z., Xu, H., 2008. Study on the spatial pattern of rainfall erosivity based on geostatistics in Hebei Province, China. Front. Agric. China 2 (3), 281–289.
Meusburger, K., Steel, A., Panagos, P., Montanarella, L., Alewell, C., 2012. Spatial and temporal variability of rainfall erosivity factor for Switzerland. Hydrol. Earth Syst. Sci. 16 (1), 167–177.
Min, S.K., Zhang, X., Zwiers, F.W., Hegerl, G.C., 2011. Human contribution to more-intense precipitation extremes. Nature 470 (7334), 378–381.
Mondal, A., Khare, D., Kundu, S., 2016. Change in rainfall erosivity in the past and future due to climate change in the central part of India. Int. Soil Water Conserv. Res. 4 (3), 186–194.
Morgan, P.R.C., 2005. Chapter 4. Erosion Hazard Assessment. Soil Erosion and Conservation, third ed. Blackwell Publishing, London, p. 67.
Nangombe, S., Zhou, T., Zhang, W., Wu, B., Hu, S., Zou, L., Li, D., 2018. Record-breaking climate extremes in Africa under stabilized 1.5 C and 2 C global warming scenarios. Nature. Clim. Change 8 (5), 375–380.
Nearing, M.A., Pruski, F.F., Oneal, M.R., 2004. Expected climate change impacts on soil erosion rates: a review. J. Soil Water Conserv. 59 (1), 43–50.
O'Gorman, P.A., Schneider, T., 2009. The physical basis for increases in precipitation extremes in simulations of 21st-century climate change. Proc. Natl. Acad. Sci. 106 (35), 14773–14777.
O'Neill, B.C., Tebaldi, C., Vuuren, D.P.V., Eyring, V., Friedlingstein, P., Hurtt, G., Sanderson, B.M., 2016. The scenario model intercomparison project (ScenarioMIP) for CMIP6. Geosci. Model Dev. 9 (9), 3461–3482.
Pimentel, D., 2006. Soil erosion: a food and environmental threat. Environ. Dev. Sustain. 8 (1), 119–137.
Pimentel, D., Harvey, C., Resosudarmo, P., Sinclair, K., Kurz, D., McNair, M., Blair, R., 1995. Environmental and economic costs of soil erosion and conservation benefits. Science 267 (5201), 1117–1123.
Qin, W., Guo, Q., Zuo, C., Shan, Z., Ma, L., Sun, G., 2016. Spatial distribution and temporal trends of rainfall erosivity in mainland China for 1951–2010. Catena 147, 177–186.
Renard, K.G., Foster, G.R., Weesies, G.A., McCool, D.K., Yoder, D.C., 1997. Predicting soil erosion by water: A guide to conservation planning with the Revised Universal Soil Loss Equation (RUSLE). Agric. Handbook 703, 25–28.
Saha, A., Ghosh, S., 2020. Relative Impacts of Projected Climate and Land Use Changes on Terrestrial Water Balance: A Case Study on Ganga River Basin. Front. Water 2, 12.
Salvi, K., Ghosh, S., Ganguly, A.R., 2016. Credibility of statistical downscaling under nonstationary climate. Clim. Dyn. 46 (5–6), 1991–2023.
Sanderson, B.M., Xu, Y., Tebaldi, C., Wehner, M., O'Neill, B., Jahn, A., Lamarque, J.F., 2017. Community climate simulations to assess avoided impacts in 1.5 and 2 C futures. Earth System. Dynamics 8 (3), 827–847.
Schleussner, C.F., Lissner, T.K., Fischer, E.M., Wohland, J., Perrette, M., Golly, A., Schaeffer, M., 2016. Differential climate impacts for policy-relevant limits to global warming: the case of 1.5 C and 2 C. Earth Syst. Dyn. 7 (2), 327–351.

SWCS, (2003). Conservation Implications of Climate Change: Soil Erosion and Runoff from Cropland.
Tarolli, P., Sofia, G., 2016. Human topographic signatures and derived geomorphic processes across landscapes. Geomorphology 255, 140–161.
Teng, H.F., Hu, J., Zhou, Y., Zhou, L.Q., Shi, Z., 2019. Modelling and mapping soil erosion potential in China. Journal of integrative agriculture 18 (2), 251–264.
Trenberth, K.E., Dai, A., Rasmussen, R.M., Parsons, D.B., 2003. The changing character of precipitation. Bull. Am. Meteorol. Soc. 84 (9), 1205–1218.
United Nations Framework Convention on Climate Change 2015 Decision 1/CP.21. The Paris Agreement.
USDA-Agricultural Research Service. (2013). Science Documentation Revised Universal Soil Loss Equation Version 2. https://www.ars.usda.gov/ARSUserFiles/60600505/RUSLE/RUSLE2_Science_Doc.pdf.
Verheijen, F.G., Jones, R.J., Rickson, R.J., Smith, C.J., 2009. Tolerable versus actual soil erosion rates in Europe. Earth Sci. Rev. 94 (1–4), 23–38.
Wang, B., Zheng, F., Guan, Y., 2016. Improved USLE-K factor prediction: A case study on water erosion areas in China. Int. Soil Water Conserv. Res. 4 (3), 168–176.
Wang, G., Fang, Q., Wu, B., Yang, H., Xu, Z., 2015. Relationship between soil erodibility and modeled infiltration rate in different soils. J. Hydrol. 528, 408–418.
Wentz, F.J., Ricciardulli, L., Hilburn, K., Mears, C., 2007. How much more rain will global warming bring? Science 317 (5835), 233–235.
Wilby, R.L., Wigley, T.M.L., 1997. Downscaling general circulation model output: A review of methods and limitations. Prog. Phys. Geogr. 21 (4), 530–548. https://doi.org/10.1177/030913339702100403.
Wischmeier, W.H., Smith, D.D., 1978. Predicting Rainfall Erosion Losses. A Guide to Conservation Planning. United States Department of Agriculture, Agricultural Handbook #537.
Wu, J., Gao, X., 2013. A gridded daily observation dataset over China region and comparison with the other datasets. Chin. J. Geophys. (in Chinese) 56, 1102–1111. https://doi.org/10.6038/cjg20130406.
Xu, Y., Gao, X., Shen, Y., Xu, C., Shi, Y., Giorgi, F., 2009. A daily temperature dataset over China and its application in validating a RCM simulation. Adv. Atmos. Sci. 26 (4), 763–772. https://doi.org/10.1007/s00376-009-9029-z.
Yang, F., Lu, C., 2015. Spatiotemporal variation and trends in rainfall erosivity in China's dryland region during 1961–2012. Catena 133, 362–372.
Yang, K., Lu, C., 2018. Evaluation of land-use change effects on runoff and soil erosion of a hilly basin—the Yanhe River in the Chinese Loess Plateau. Land Degrad. Dev. 29 (4), 1211–1221.
Yang, Y., Tang, J., Wang, S., Liu, G., 2018. Differential impacts of 1.5 and 2 C warming on extreme events over China using statistically downscaled and bias-corrected CESM low-warming experiment. Geophys. Res. Lett. 45 (18), 9852–9860.
Zhang, W., Zhou, T., 2019. Significant increases in extreme precipitation and the associations with global warming over the global land monsoon regions. J. Clim. 32 (24), 8465–8488.
Zhang, W., Zhou, T., 2020. Increasing impacts from extreme precipitation on population over China with global warming. Sci. Bull. 65 (3), 243–252.
Zhang, W., Zhou, T., Zou, L., Zhang, L., Chen, X., 2018. Reduced exposure to extreme precipitation from 0.5 C less warming in global land monsoon regions. Nat. Commun. 9 (1), 1–8.
Zhang, W.B., Xie, Y., Liu, B.Y., 2002. Rainfall erosivity estimation using daily rainfall amounts. Sci. Geogr. Sin. 22, 705–711 (In Chinese).
Zhang, X.C., 2007. A comparison of explicit and implicit spatial downscaling of GCM output for soil erosion and crop production assessments. Clim. Change 84 (3), 337–363.
Zhang, X.C., Nearing, M.A., 2005. Impact of climate change on soil erosion, runoff, and wheat productivity in central Oklahoma. Catena 61 (2–3), 185–195.
Zhao, S., Zhou, T., 2019. Are the observed changes in heat extremes associated with a half-degree warming increment analogues for future projections? Earth's Future 7 (8), 978–992.
Zhou, M., Zhou, G., Lv, X., Zhou, L., Ji, Y., 2019. Global warming from 1.5 to 2° C will lead to increase in precipitation intensity in China. Int. J. Climatol. 39 (4), 2351–2361.
Zhu, Z., Yu, B., 2015. Validation of rainfall erosivity estimators for mainland China. Trans. ASABE 58 (1), 61–71.